Effect of Alkyl Side Chains of Conjugated Polymer Donors on the Device Performance of Non-Fullerene Solar Cells

Dongdong Xia,[†] Yang Wu,[‡] Qiang Wang,[§] Andong Zhang,[†] Cheng Li,[*,†] Yuze Lin,[||] Fallon J. M. Colberts,[§] Jacobus J. van Franeker,[§] René A. J. Janssen,[§] Xiaowei Zhan,[||] Wenping Hu,[†] Zheng Tang,[*,⊥] Wei Ma,[*,‡] and Weiwei Li[*,†]

[†]Beijing National Laboratory for Molecular Sciences, CAS Key Laboratory of Organic Solids, Institute of Chemistry, Chinese Academy of Sciences, Beijing 10090, P. R. China

[‡]State Key Laboratory for Mechanical Behavior of Materials, Xi'an Jiaotong University, Xi'an 710049, P. R. China
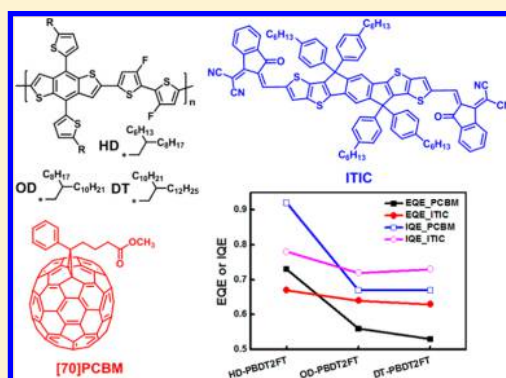
[§]Molecular Materials and Nanosystems & Institute for Complex Molecular Systems, Eindhoven University of Technology, P.O. Box 513, Eindhoven 5600 MB, The Netherlands

[||]Department of Materials Science and Engineering, College of Engineering, Peking University, Beijing 100871, P. R. China

[⊥]Institut für Angewandte Photophysik, Technische Universität Dresden, George-Bähr-Straße 1, Dresden 01069, Germany

S *Supporting Information*

ABSTRACT: The influence of the chemical structure of conjugated polymers on the nanophase separation and device performance in fullerene-based solar cells has been widely studied, while this is less investigated in non-fullerene solar cells. In this work, we design three conjugated polymers with different length of side chains, and we find that the length of side chains has little influence on the quantum efficiencies of non-fullerene solar cells. As a comparison, the length of side chains has a significant effect on the quantum efficiencies of fullerene-based solar cells. This indicates that morphology of the blended thin films in non-fullerene solar cells is rather independent of the length of the donor side chains, and the mechanism for morphology evolution in the non-fullerene system is completely different from that in the fullerene system. Our conclusion is confirmed by a variety of advanced characterization techniques. The studies reveal that in blended thin films based on the non-fullerene material the donor polymers with different side chains have a similar coherence length of $\pi-\pi$ stacking, crystal size and domain purity, giving rise to similar internal quantum efficiency and power conversion efficiency of the solar cells.

1. INTRODUCTION

Non-fullerene organic solar cells (NFOSCs) have emerged as a promising alternative to fullerene-based solar cells in recent years.[1−7] By exploring numerous conjugated electron acceptor materials,[8−31] NFOSCs with power conversion efficiencies (PCEs) exceeding 11% have recently been realized.[31] The PCE of NFOSCs is now comparable to that of fullerene-based solar cells.[32] Studies also revealed that NFOSCs have an excellent stability at high temperatures[31] and bending tests,[33] which is highly desired for large-area roll-to-roll manufacturing. High performance solar cells also offer the opportunity to study the effect of non-fullerene acceptors on the morphology, charge generation process, and device performance, which is helpful for the design of new acceptors for highly efficient solar cells.

The photoabsorbing layer in bulk-heterojunction (BHJ) solar cells consists of an electron donor and an electron acceptor. The nanoscale phase separation between the donor and the acceptor has a crucial influence on the photon to electron conversion process, i.e., exciton diffusion to the interface of donor and acceptor, exciton dissociation, and charge carrier

separation, transport, and extraction.[34] In fullerene-based solar cells, the relation between conjugated materials, morphology, and device performance has been widely studied.[35] For instance, by introducing heteroatoms such as fluorine,[36−39] silicon,[40] and selenium[41] in the backbone, the crystalline properties of the conjugated polymers can be improved, resulting in a high degree of orientation of the conjugated backbone[42] and optimized domain size[37] in blended thin films. Similar effects on the morphology of the photoactive layers were observed when manipulating the branching point of alkyl side chains on the conjugated polymers.[43] In our previous work, we showed that by decreasing the length of the side chains in a crystalline conjugated polymer, the width of the fibrillar microstructures in the blended thin films was reduced, which was found to facilitate exciton dissociation and led to enhanced solar cell performance.[44] The morphology of the
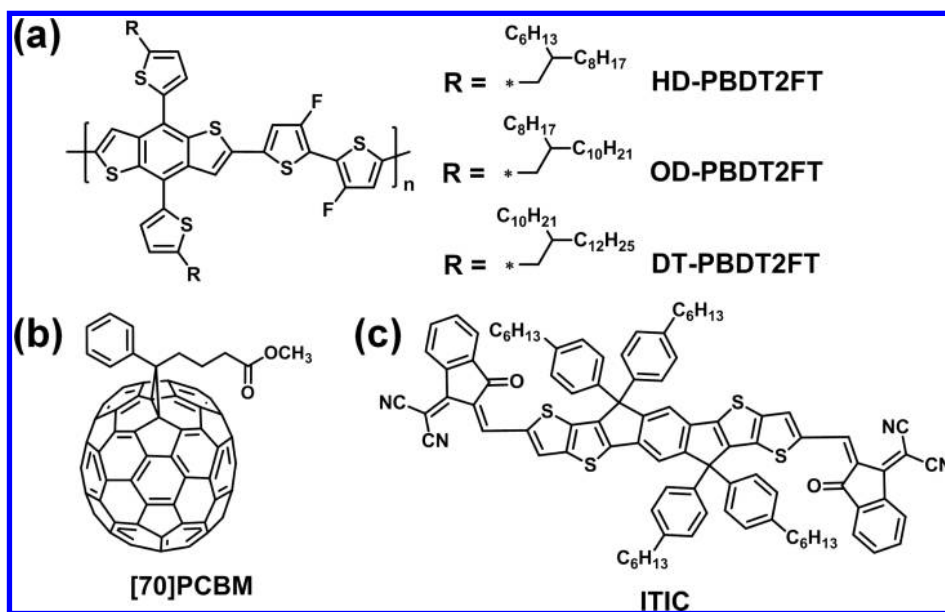
Figure 1. Chemical structures of (a) conjugated polymers HD-, OD-, and DT-PBDT2FT. (b) [70]PCBM. (c) Non-fullerene electron acceptor ITIC.

active layer has also been investigated for NFOSCs, with special focus on the improvement in microphase separation to reduce charge carrier recombination and enhance the fill factor (FF) and performance of solar cells.[45,46] However, the effect of the chemical structure of conjugated materials on device performance of efficient NFOSCs needs to be further investigated.
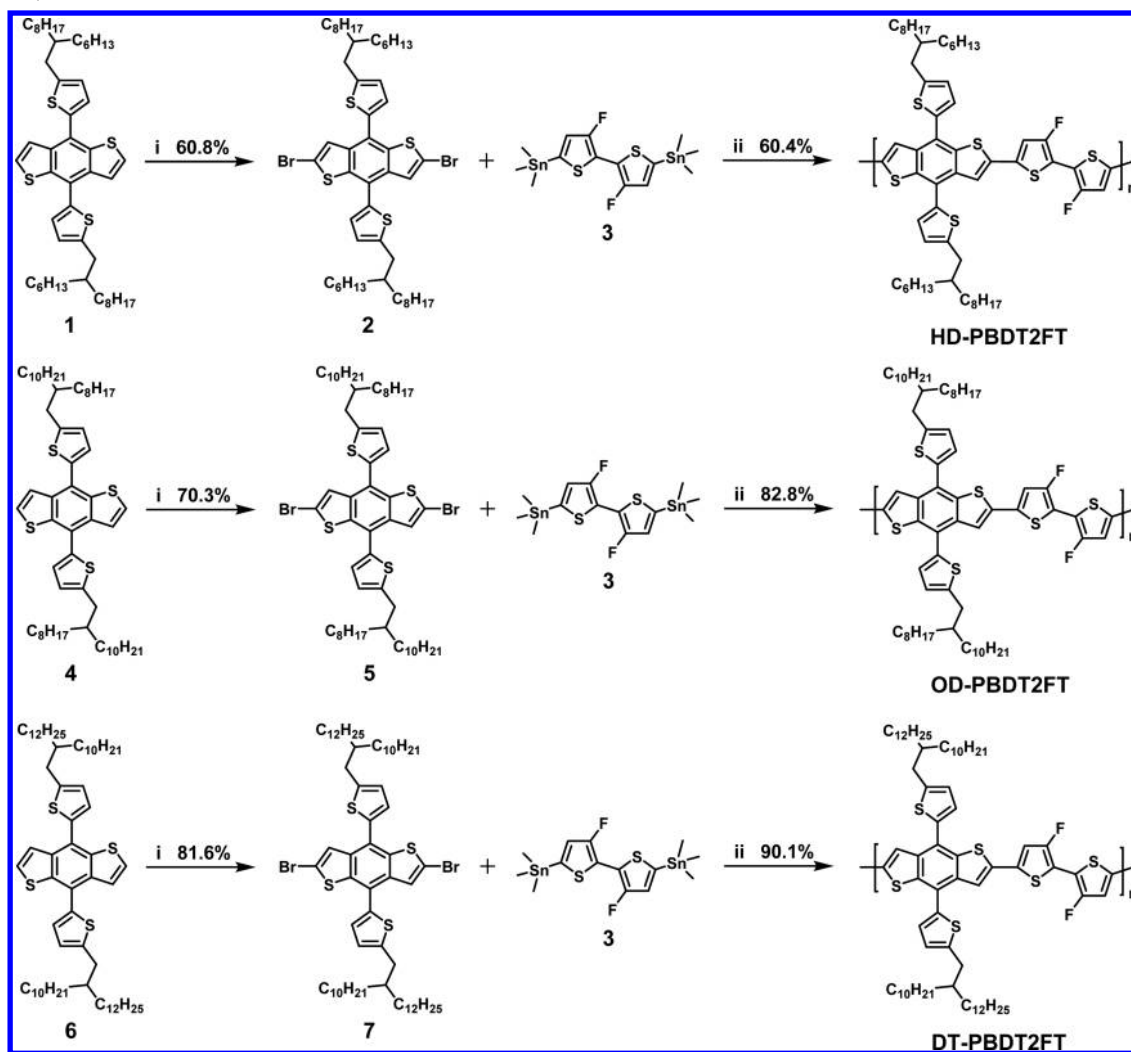
In this work, we are dedicated to investigate the relation between the chemical structure of the donor and the device performance in NFOSCs. The study starts with designing three crystalline conjugated polymers containing alkylthienylbenzodithiophene (TBDT) and fluoro-based bithiophene (2FT) units, in which the length of the side chains varies from 2′-hexyldecyl (HD) to longer 2′-octyldodecyl (OD) and 2′-decyltetradecyl (DT) (Figure 1a). These polymers are used as the electron donors in combination with 3,9-bis(2-methylene-(3-(1,1-dicyanomethylene)indanone)-5,5,11,11-tetrakis(4-hexylphenyl)dithieno[2,3-d:2′,3′-d′]-s-indaceno[1,2-b:5,6-b′]-dithiophene (ITIC) (Figure 1c) as the electron acceptor in bulk heterojunction solar cells. The highest PCE of 8.7% is achieved for the polymer with the HD side chain. Importantly, we demonstrate that the length of the side chain of the donor material has little influence on the internal quantum efficiency (IQE) of the ITIC solar cells, whereas for the solar cell with a fullerene acceptor, the IQE depends strongly on the length of the donor side chain. We further combine real space and reciprocal space techniques such as transmission electron microscopy (TEM), grazing-incidence wide-angle X-ray scattering (GIWAXS), and resonant soft X-ray scattering (R-SoXS) to investigate the blend thin films. We show that a similar nanophase separation is obtained when ITIC is mixed with the donors containing different side units but that a completely different result is obtained for the PCBM-based systems, consistent with the differences in the IQE.

2. RESULTS AND DISCUSSION

Synthesis of the Conjugated Polymers. The conjugated polymers studied in this work contain FBDT and 2FT units in the conjugated backbone. It is interesting to elucidate the donor and acceptor strength of FBDT and 2FT units in the

conjugated polymers. We apply density function theory (DFT) calculations to analyze the frontier orbital energies of TBDT, 2FT, homopolymer based on the two units, and PBDT2FT (Tables S1 and S2, Supporting Information).[47,48] TBDT and 2FT units perform highest occupied molecular orbital (HOMO) and lowest unoccupied molecular orbital (LUMO) levels of −5.14 eV (−1.33 eV) and −5.59 eV (−1.30 eV) (Table S1). 2FT-based homopolymer shows similar HOMO level (−4.94 eV) with TBDT-based homopolymer (−4.84 eV), while it performs significant low-lying LUMO of −2.56 eV compared to TBDT-based homopolymer (−2.18 eV) (Table S2). This indicates that 2FT is a weak acceptor compared to the TBDT unit, which can be further confirmed by similar LUMO level of PBDT2FT segment (−2.40 eV) with 2FT-based homopolymer.[49] This "donor−weak acceptor" method can likely be used to design conjugated polymers with deep HOMO and LUMO levels since the HOMO level can be controlled by the donor part, while the LUMO level is related to the weak acceptor.[48]

The synthetic procedures for the monomers and polymers are presented in Scheme 1. The dibromo-monomers 2, 5, and 7 are synthesized from the precursors 1, 4, and 6 by using CBr₄ as bromination agent. The polymers HD-, OD-, and DT-PBDT2FT were synthesized via Stille polymerization, in which a Pd₂(dba)₃/PPh₃ (1:4) catalyst and toluene/DMF (10:1) solvent mixture were used. Gel permeation chromatography (GPC) with o-DCB as eluent at 140 °C was used to determine the molecular weight of the polymers, as shown in Figure S1. HD-PBDT2FT shows a number-average molecular weight (M_n) of 31.6 kg mol⁻¹ with polydispersity (PD) of 2.92, while OD- and DT-PBDT2FT possess a high M_n of 77.2 and 107.6 kg mol⁻¹. We note that HD-PBDT2FT precipitates after 30 min during the polymerization reaction, but OD-PBDT2FT and DT-PBDT2FT result in a gel-like solution in toluene/DMF even after 2 h polymerization. In the GPC of HD-PBDT2FT, a bimodal distribution is observed. Next to the main peak a shoulder at lower molecular weight is present. This may be related to the observed precipitation of HD-PBDT2FT during polymerization.

Scheme 1. Synthetic Routes of HD-, OD-, and DT-PBDT2FT[a]

[a]Reagents and conditions: (i) *n*-butyllithium, RT, 3 h; CBr$_4$ in THF, −78 °C, warm to RT, overnight; (ii) Stille polymerization by using Pd$_2$(Dba)$_3$/PPh$_3$ in toluene/DMF (10:1, v/v) at 115 °C.

Absorption Spectra and Energy Levels. The three polymers have similar absorption spectra in chlorobenzene (CB) solution and in thin film (Figure 2). The optical band gap
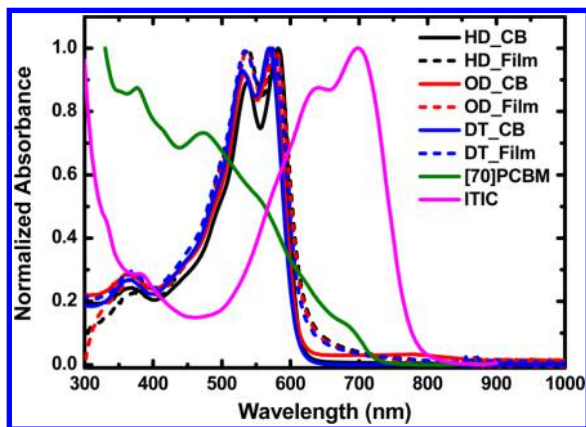

Figure 2. (a) Absorption spectra of HD-, OD-, and DT-PBDT2FT in chlorobenzene solution and thin film. The absorption spectra of [70]PCBM and ITIC thin films are also included.

(E_g) is 2.05 eV in solution and 2.00 eV in thin film (Table 1). The absorption spectra of [70]PCBM and ITIC in thin films are also present in Figure 2 for comparison. [70]PCBM strongly absorbs in the range of 400−500 nm, while ITIC strongly absorbs between 600 and 800 nm ($E_g \sim 1.59$ eV). The polymers and ITIC possess complementary absorption in the visible and near-infrared region, which is beneficial to cover a significant fraction of the solar spectrum. The polymers have similar energy levels with HOMO between −5.50 and −5.57 eV and the LUMO levels between −3.50 and −3.57 eV, as determined by cyclic voltammetry measurements (Figure S2 and Table 1). To compare, [70]PCBM and ITIC have HOMO levels of −5.99 and −5.50 eV, respectively, and the LUMO levels are −4.00 and −3.90 eV. The LUMO offset between the polymers and acceptors is above 0.3 eV, while the HOMO offset between PBDT2FT and ITIC is very low. A similar phenomenon was observed in other ITIC-based systems.[31] It is generally accepted that the energy offset between the LUMO levels must be 0.3 eV or higher for efficient separation of charge carriers, although exceptions are known.[50] However, charge separation at a very low HOMO offset has not been reported and requires more detailed investigation.

Table 1. Molecular Weight, Optical, Electrochemical, and Charge Transport Properties of the PBDT2FTs

polymer	M_n (kg mol^{-1})	PDI	E_g^{film} (eV)	E_{HOMO}^a (eV)	E_{LUMO}^b (eV)	μ_h (cm^2 V^{-1} s^{-1})
HD-PBDT2FT	31.6	2.92	2.00	−5.50	−3.50	0.79
OD-PBDT2FT	77.2	1.88	2.00	−5.52	−3.52	0.091
DT-PBDT2FT	107.6	2.24	2.00	−5.57	−3.57	0.022
[70]PCBM				−5.99	−4.00	
ITIC			1.59	−5.50	−3.91	

^{a}Determined by $-4.80 - E_{ox}$. $^c E_{LUMO}$ is calculated as $E_{HOMO} + E_g^{film}$.
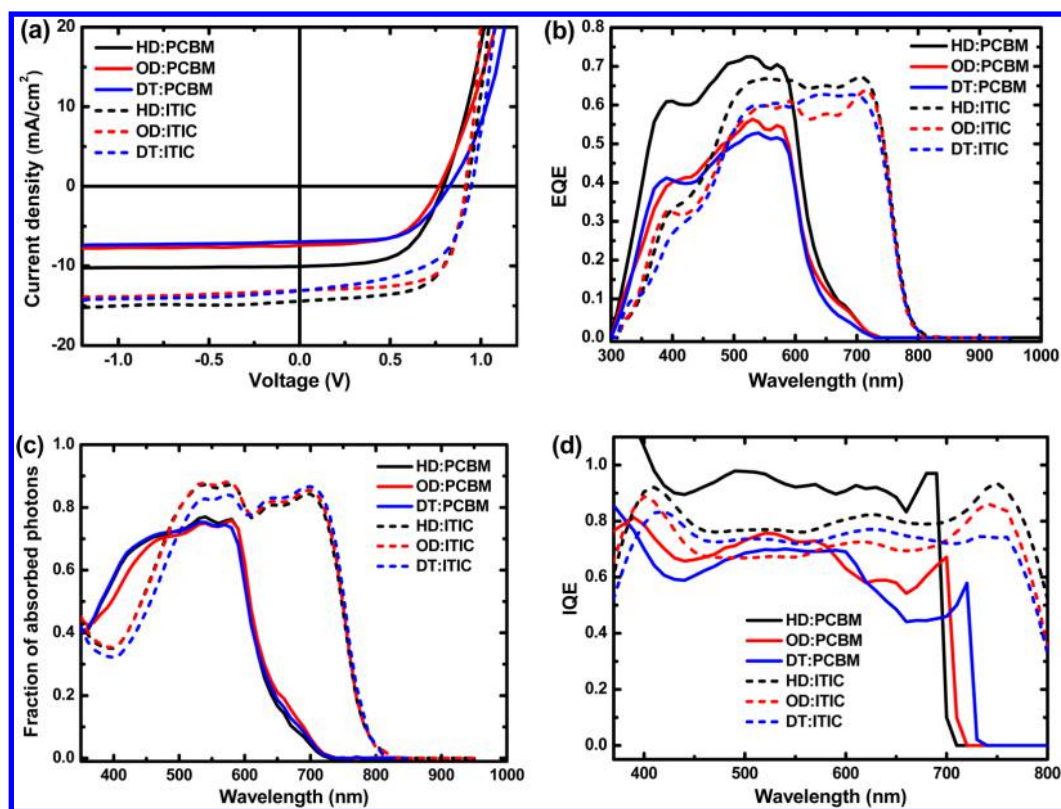

Figure 3. (a) $J-V$ characteristics of PBDT2FT:ITIC (dashed lines) and PBDT2FT:[70]PCBM (solid lines) solar cells under simulated solar illumination. (b) EQE of the solar cells. (c) Fraction of photons absorbed in the photoactive layers (80 and 60 nm for PCBM and ITIC-based cells), calculated with a transfer matrix model. (d) Calculated IQE spectra.

Charge Transport Properties. Charge transport plays an important role in organic solar cells, in which a high hole mobility of donor polymer is helpful for charge exaction and reducing charge recombination. Here, we use field-effect transistors (FETs) to determine the charge transport properties of PBDT2FTs. The hole mobilities of these polymers are strongly related to thermally annealed temperatures, as present in Table S3. The transfer and output curves are shown in Figure S3, and the key parameters are summarized in Table 1. The polymer HD-PBDT2FT exhibits a hole mobility (μ_h) of 0.79 cm^2 V^{-1} s^{-1}, while the mobilities of OD- and DT-PBDT2FT are 0.091 and 0.022 cm^2 V^{-1} s^{-1}, respectively. The low mobility of the PBDT2FT with the longer OD and DT side chains may originate from a change of molecular packing from "edge-on" to "face-on", which will be discussed below in more detail (Figure 6a−c). It is desired to mention that the charge transport direction in FETs is parallel to the substrate, while in PSCs it is vertical to the substrate. The detailed charge transport properties of blended thin films in solar cells will be discussed below by space charge limited current (SCLC) measurement.

Solar Cells Performance. ITIC and its derivatives based on indacenodithiophene as core and 2-(3-oxo-2,3-dihydro-inden-1-ylidene)malononitrile as end group were reported by Zhan et al. as promising acceptor materials for non-fullerene solar cells due to their strong absorption in the near-infrared region and LUMO levels similar to PCBM.[19−31] PBDT2FT:[70]PCBM cells exhibit better optimized device performance in a regular device configuration with ITO/PEDOT bottom and LiF/Al top electrodes, while PBDT2FT:ITIC cells have higher PCEs in an inverted cell structure with ITO/ZnO bottom and MoO$_3$/Ag top electrodes (parts 7 and 8, Supporting Information) because regular PBDT2FT:ITIC solar cells show an S-shaped current density−voltage ($J-V$) curve (Figure S5), indicating a non-Ohmic contact. The processing conditions for the active layer, such as the choice of solvent, the amount of 1,8-iodooctane (DIO) as solvent additive, the donor to acceptor ratio, and the thickness of the active layer were systematically optimized to achieve high photovoltaic performance. Results are shown in Tables S4−S9 and Figures S4−S5 in the Supporting Information. The solar cell parameters, including short-circuit current densities (J_{sc}),

Table 2. Device Performance of Optimized Solar Cells of PBDT2FT with [70]PCBM or ITIC as Acceptor

	solvent	J_{sc}[a] (mA cm^{-2})	V_{oc} (V)	FF	PCE (%)	EQE$_{max}$
HD-PBDT2FT:PCBM[b]	CB/DIO (2.5%)	10.1	0.79	0.58	4.6	0.73[d]
OD-PBDT2FT:PCBM[b]	CB/DIO (5%)	7.4	0.77	0.58	3.4	0.56[d]
DT-PBDT2FT:PCBM[b]	CB/DIO (5%)	7.0	0.83	0.60	3.4	0.53[d]
HD-PBDT2FT:ITIC[c]	CB/DIO (0.2%)	14.4	0.92	0.65	8.7	0.67[e]
OD-PBDT2FT:ITIC[c]	CB/DIO (0.2%)	13.1	0.92	0.69	8.3	0.64[e]
DT-PBDT2FT:ITIC[c]	CB/DIO (0.2%)	13.1	0.95	0.57	7.0	0.63[e]

[a]J_{sc} are calculated by integrating the EQE spectrum with the AM1.5G spectrum. [b]Weight ratio of polymer to [70]PCBM is 1:1.5, and the thickness of the active layers is 80 nm. The solar cells have a regular cell configuration. [c]Weight ratio of polymer to ITIC is 1:1, and the thickness of the active layer is 60 nm. The solar cells have an inverted cell configuration. [d]Maximum EQE found at the wavelength of 530 nm. [e]Maximum EQE found at the wavelength region >630 nm. This table presents the best PCEs for each cell.

open circuit voltage (V_{oc}), FF, and PCEs, were first measured under the AM1.5G spectrum from solar simulator. In order to eliminate the spectral mismatch between the solar simulator and natural sunlight from AM1.5G, we intend to use the J_{sc} determined by integrating the EQE with the AM1.5G (100 mW cm^{-2}) spectrum, so that PCEs can be recalculated by using J_{sc}, V_{oc}, and FF.[51] The J_{sc}s and PCEs from the two methods are also present in Tables S4−S9 for comparison, showing the derivation within 10%. The J−V characteristics and external quantum efficiency (EQE) of the optimized solar cells are shown in Figure 3 and Table 2, and the statistic PCEs are present in Figure S6.

For PBDT2FTs:[70]PCBM solar cells, the best performance is achieved when the active layer is spin-coated from CB with 2.5% or 5% DIO. For these fullerene-based solar cells, the highest PCE of 4.6% is obtained when HD-PBDT2FT is used as the donor material (Table 2). The PCE of the solar cell based on OD- or DT-PBDT2FT is lower (3.4%), mainly due to a lower J_{sc}, compared to that of the solar cell based on HD-PBDT2FT. The overall low J_{sc} of the fullerene-based solar cells is reflected by the narrow spectral response from 300 to 650 nm. The maximum EQE reaches up to 0.73 (Figure 3b) for HD-PBDT2FT-based cells, indicating that the photon to electron conversion is already highly efficient and the photovoltaic performance is limited by the narrow absorption spectrum, the moderate FF, and the low V_{oc} compared to the optical band gap. The maximum EQE is reduced to 0.56 and 0.53 for OD- and DT-PBDT2FT with longer side chains. The results reveal that the length of side chain of donor polymer has a strong effect on the device performance of the fullerene-based solar cells, which corresponds well with our previous observation.[44]

We then employed ITIC as the electron acceptor. The highest PCE (8.7%) is obtained from the solar cell based on PBDT2FT:ITIC with a D/A ratio of 1:1. The optimal DIO content is found to be 0.2%, and the optimized thickness of the active layer is 60 nm. The PCE of OD-PBDT2FT:ITIC cell is only slightly lower (8.3%), with J_{sc} of 13.1 mA cm^{-2} and a high FF of 0.69. For the solar cell based on DT-PBDT2FT with the longest side chain, the PCE is reduced to 7.0%, mostly due to the low FF (0.57). Note that the J_{sc}s of these non-fullerene solar cells are very similar regardless of the length of the side chain of the donor material. The high J_{sc}s of ITIC-based cells are related to the broad EQE spectrum with a strong photoresponse between 300 and 800 nm. The maximum EQEs of the cells based on HD-, OD-, and DT-PBDT2FT are 0.67, 0.64, and 0.63.

The effects of the length of the donor side chain on the performance of the fullerene-based and ITIC-based solar cells

are different, which indicates that the relation between the length of the donor side chain and the active layer morphology is different for the two different systems. This is supported by their different IQE (Figure 3d). The IQE of the solar cell is estimated by taking the ratio between the measured EQE and the fraction of photons absorbed in the photoactive layer predicted with a transfer matrix model based on the optical constants of the materials. The predicted fraction of photons absorbed in the active layer is about 80% (Figure 3c), which gives rise to IQEs over 60% for all of the solar cells based on either PCBM and ITIC. For PCBM-based solar cells, the IQE spectra are nonflat, most likely due to a small inconsistency in the morphology of the BHJ layer which could be different in the thin film (for determination of the optical constants) and in the device. Nevertheless, the average IQE (Table S10) is found to be strongly dependent on the length of the side chain of the donor material. It should be noted that extraction of photocurrent from all of the solar cells studied here is virtually independent of the electric field at short circuit. This indicates that losses in IQE are due to inefficient dissociation of excitons. Therefore, the difference in IQE obtained from the fullerene-based solar cells is directly related to a difference in the degree of phase separation between the donor and fullerene in the active layer, which is a result of the change of the length of the donor side chain.

For ITIC-based solar cells, we determined very similar IQE values and similar J_{sc} (Table S10). This suggests that the length of side chain on the donor polymer has little influence on the morphology of the ITIC-based solar cells, while this influence is significant in the PCBM-based cells. The IQE spectra are relatively flat, suggesting that generation and extraction of photogenerated charge carriers are equally efficient in the PBDT2FT and ITIC phases.

We also measured the hole and electron (μ_e) mobilities in the BHJ systems by the SCLC method (Table 3 and Figure S7). The polymers and the acceptors exhibit mobilities of

Table 3. Hole and Electron Mobilities from SCLC Measurements[a]

	μ_h [cm^2 V^{-1} s^{-1}]	μ_e [cm^2 V^{-1} s^{-1}]	μ_h/μ_e
HD-PBDT2FT:PCBM	2.2×10^{-5}	2.3×10^{-5}	0.96
OD-PBDT2FT:PCBM	4.0×10^{-6}	3.4×10^{-5}	0.12
DT-PBDT2FT:PCBM	5.0×10^{-6}	3.7×10^{-6}	1.35
HD-PBDT2FT:ITIC	8.0×10^{-6}	4.8×10^{-5}	0.17
OD-PBDT2FT:ITIC	7.4×10^{-6}	6.6×10^{-7}	11.2
DT-PBDT2FT:ITIC	1.4×10^{-5}	2.6×10^{-6}	5.38

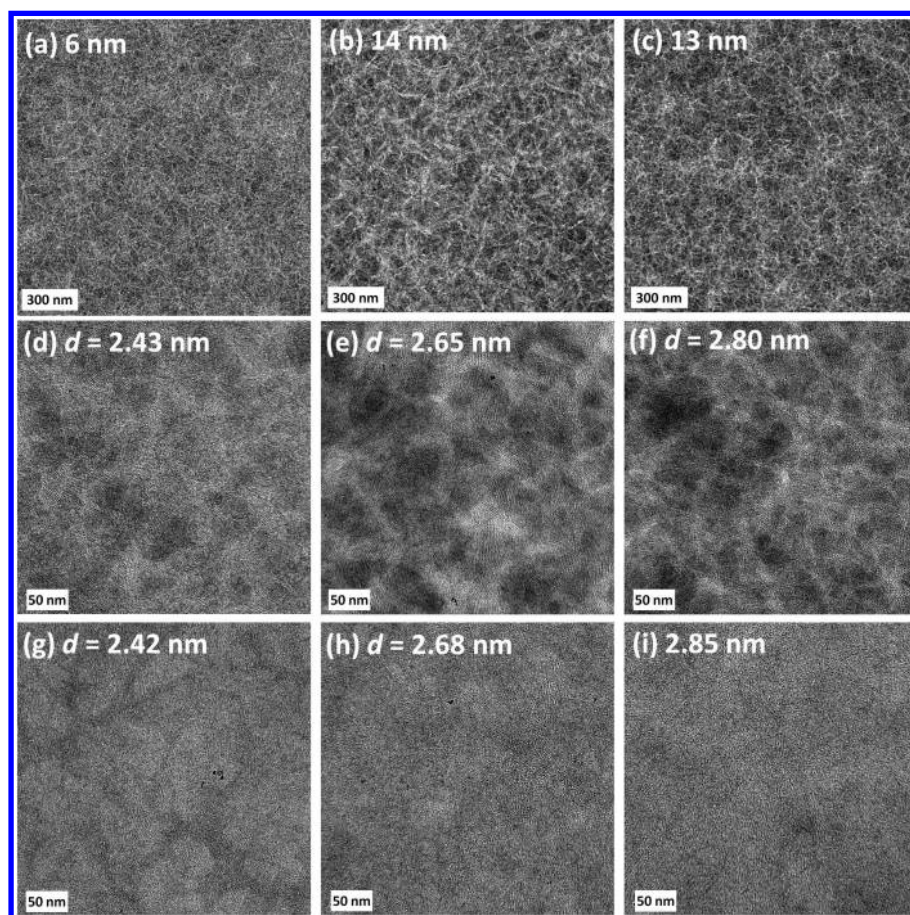[a]The thickness for PCBM-based active layers is around 80 nm. The thickness for ITIC-based active layers is around 60 nm.

Figure 4. Bright field TEM images (1.2×1.2 μm^2 and 225×225 nm^2) of the blended thin films: (a, d) HD-PBDT2FT:[70]PCBM; (b, e) OD-PBDT2FT:[70]PCBM; (c, f) DT-PBDT2FT:[70]PCBM; (g) HD-PBDT2FT:ITIC; (h) OD-PBDT2FT:ITIC; (i) DT-PBDT2FT:ITIC. Calculated *d*-spacing values are also included.

10^{-7}–10^{-5} cm^2 V^{-1} s^{-1}, which are slightly lower than that of the previously reported high performance ITIC-based cells.[31] In general, the ratio of μ_h and μ_e is related to the charge transport, in which the ratio close to 1 indicates that hole and electron can be equally generated at electrode so as to reduce charge recombination. This is helpful for enhancing J_{sc} and FF. Unfortunately, the SCLC mobilities in our measurement are difficult to relate to the current and FF, as present in Table 3 with ruleless μ_h/μ_e.

Morphology Analyzed by TEM Images. To investigate the effect of the length of the donor side chain on the morphology of the active layers based on fullerene and ITIC, the photoactive layers were analyzed by bright-field TEM, as shown in Figure 4. Clear fibrillar structures are observed in the PCBM-containing films, and the width of the fibril depends strongly on the length of the donor side chain. The fibril width increases from 6 to 14 and 13 nm for HD-, OD-, and DT-PBDT2FT:PCBM systems, respectively (Figure 4a−c). In the thicker fibrils, the photogenerated excitons do not have the time to efficiently diffuse to a D/A interface, which in turn limits the IQE and EQE of the fullerene solar cells based on OD- and DT-PBDT2FT. We failed to observe polymer fibers in ITIC-based thin films (Figure S8), which is similar to other non-fullerene systems.[52] This may be caused by the low contrast between the donor polymers and ITIC in the TEM experiment. However, clear lattice fringes related to the semicrystalline nature of the polymers can be observed at higher magnification in the TEM images of PCBM- and ITIC-

based thin films (Figure 4d−i). The *d*-spacing of the lattice fringes for these active layers is found to be 2.43, 2.65, and 2.80 nm for HD-, OD-, and DT-PBDT2FT mixed with PCBM. The *d*-spacing corresponds to the lamellar stacking of the alkyl side chains, and it is further confirmed by the GIWAXS measurements below. These results indicate that in both PCBM- and ITIC-based thin films the conjugated polymers are semicrystalline.

GIWAXS and R-SoXS Analysis. To further elucidate the effect of the length of the donor side chain on the morphology of the active layer based on ITIC and PCBM, we performed GIWAXS (Figure 5) and R-SoXS (Figure 6), and the results are summarized in Table 4. The pure HD-PBDT2FT polymer shows highly ordered crystalline properties, as evidenced by the series of diffraction peaks (up to the fourth order) associated with the lamellar packing of the alkyl chains. The (010) diffraction peak in the in-plane direction is also observed, indicating a strong $\pi-\pi$ stacking (spacing: ca. 0.36 nm). Therefore, HD-PBDT2FT shows preferentially "edge-on" orientation, and the $\pi-\pi$ stacking direction of the conjugated polymer is parallel to the substrate. Interestingly, PBDT2FT with longer side chains of OD and DT exhibit preferentially "face-on" orientation, where the lamellar stacking (100) peaks are clearly observed in the in-plane direction and the $\pi-\pi$ stacking of (010) peaks present in the out-of-plane direction. The *d*-spacing of (100) peaks for HD-, OD-, and DT-PBDT2FT is 2.44, 2.63, and 2.85 nm, which is consistent with the *d*-spacing measured from TEM images. The results confirm
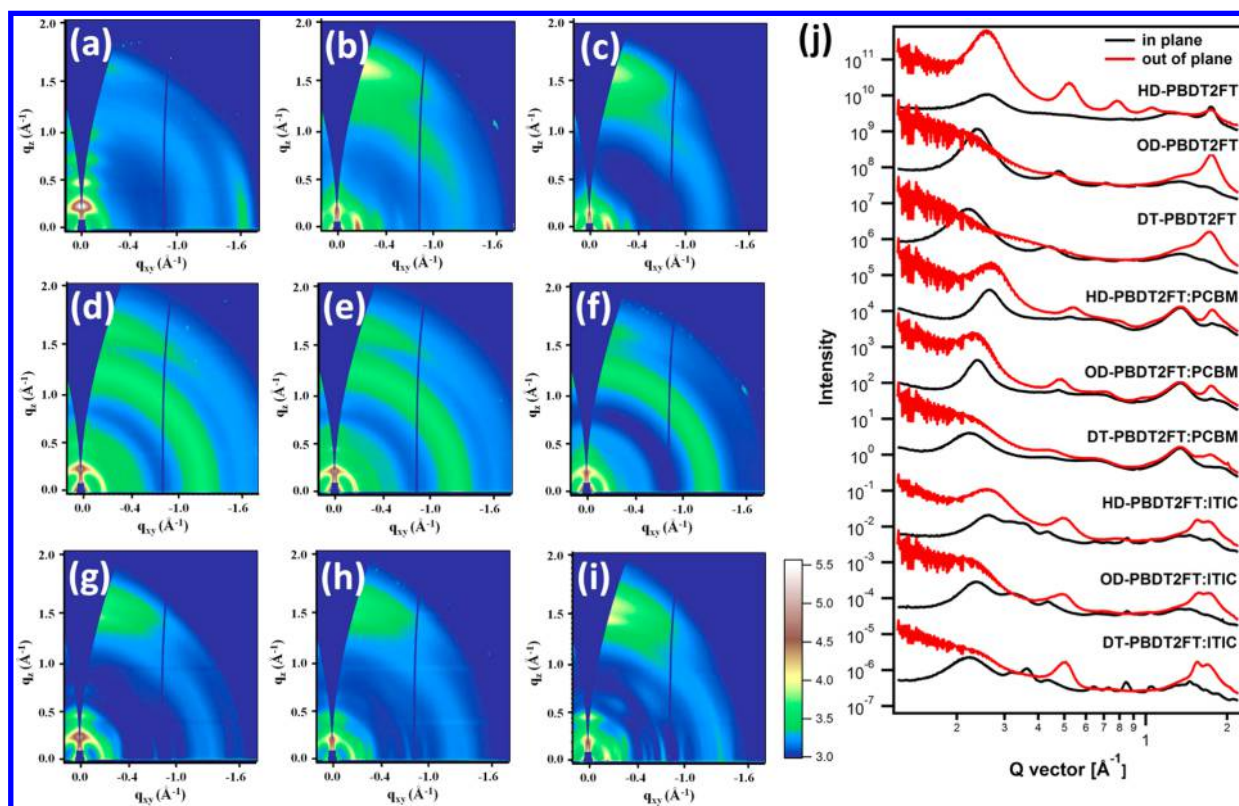
Figure 5. 2D-GIWAXS images of (a–c) pure polymer, (d–f) polymers blended with PCBM, and (g–i) polymers blended with ITIC. (a, d, g) HD-PBDT2FT. (b, e, h) OD-PBDT2FT. (c, f, i) DT-PBDT2FT. (j) Out-of-plane and in-plane cuts of the corresponding 2D-GIWAXS patterns. The pure polymer thin films were spin-coated from o-DCB and thermally annealed at 90 °C for 10 min. Polymer:PCBM (1:1.5) thin films were fabricated from CB/DIO (2.5% or 5%). Polymer:ITIC (1:1) thin films were fabricated from CB/DIO (0.2%).

Table 4. Crystallographic Parameters of the Pure Polymer and Blend Thin Films[a]

	IP (100)		OOP (010)			
	d-spacing [nm]	CL [nm]	d-spacing [nm]	CL [nm]	domain size (nm)	domain purity
HD-PBDT2FT	2.44	9.6	0.36	3.4		
OD-PBDT2FT	2.63	16.8	0.36	3.6		
DT-PBDT2FT	2.85	12.2	0.36	2.6		
HD-PBDT2FT:PCBM	2.38	14.6	0.36	3.8	20	0.49
OD-PBDT2FT:PCBM	2.64	17.1	0.36	3.8	30	0.48
DT-PBDT2FT:PCBM	2.82	10.1	0.36	2.2	22	0.43
HD-PBDT2FT:ITIC	2.41	10.5	0.37	2.8	22	1
OD-PBDT2FT:ITIC	2.67	11.3	0.36	2.8	22	0.70
DT-PBDT2FT:ITIC	2.83	9.3	0.37	2.9	21	0.63

[a]OOP: out-of-plane; IP: in-plane; CL: coherence length.

that the lattice fringes observed in the TEM images correlate with the lamellar stacking of alkyl side chains. The d-spacing of (010) peaks is around 0.36 nm for these polymers, indicating that the length of the side chains has little influence on the π−π stacking of the polymers.

We further analyze the crystalline properties of blended thin films. The d-spacing of (100) and (010) peaks in the blended thin films are similar to those in the pure polymer films. The scattering profile in the out-of plane direction is always much stronger than that in the in-plane direction, which indicates "face-on" orientation. By analyzing the diffraction patterns, we find that for PCBM-based thin films, the intensity of (010) peak is gradually reduced upon increasing the length of donor side chain (Figure 5d−f,j), while the intensity of (010) peaks is similar for these ITIC-based thin films. A similar phenomenon

is observed for the (100) peaks in the out-of-plane direction. The coherence length (CL) for these polymer thin films is shown in Table 4. In PCBM-based cells, the CL of the HD- and OD- PBDT2FT (010) peaks is 3.8 nm. The CL of DT-PBDT2FT with the longest side chain is however significantly shorter (2.2 nm). In the ITIC-based films, a similar CL of (010) peaks is found for HD-, OD-, and DT- PBDT2FT, which confirms that the π−π stacking of the polymers mixed with ITIC does not depend strongly on the length of the donor side chain.

The phase separation of the blended thin films is further investigated by the contrast-enhanced technique R-SoXS, which is based on enhanced contrast between different organic components and provides information regarding the characteristic mode length (domain size) and average compositional

G

fluctuation (domain purity). Figure 6 shows the scattering profile of the blends at 284.2 eV. The scattering intensities of
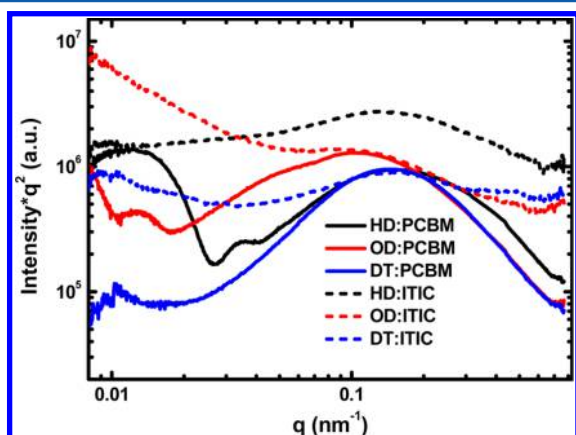

Figure 6. R-SoXS scattering profiles at 284.2 eV of the polymers blended with PCBM and ITIC.

ITIC-based blends and PCBM-based blends are normalized by the materials optical contrast. A mode domain size of 20 nm is obtained for the HD-PBDT2FT:PCBM blend film. For the OD-PBDT2FT:PCBM blend, the domain size is about 30 nm, and for DT-PBDT2FT with the longest side chain, the mode domain size was 22 nm. It is further noted that the HD-PBDT2FT:PCBM blend shows higher scattering intensity at the range of the high q, which indicates that there are more small domains distributed in the HD-PBDT2FT:PCBM blend films compared to that in the OD- or DT-PBDT2FT:PCBM blends. Smaller domains are beneficial to the exciton dissociation, which leads to the higher J_{sc} of the fullerene solar cell based on HD-PBDT2FT. For ITIC-based blend films, the dominant domain size (22 nm) is very similar regardless of the length of the donor side chain; meanwhile, the scattering distribution in the high q is higher for HD-PBDT2FT:ITIC blend films, which gives rise to the highest J_{sc} in these three ITIC-based cells.

In addition, the relative domain purity can be determined by integrating the profiles over q. The higher the total scattering intensity is, the purer the domains are. It is obvious that the ITIC-based films exhibit higher domain purity than the PCBM-based blend films. The relative domain purities of all six blends are listed in Table 4. The purer domains reduce the rate of bimolecular recombination. This explains why the relative higher FF for ITIC-based cells is obtained compared to PCBM-based cells.

3. CONCLUSIONS

In conclusion, three conjugated polymers containing TBDT and 2FT units were synthesized and used in organic solar cells to study the effect of the length of donor side chain on the device performance of PCBM- and ITIC-based solar cells. We found that the internal quantum efficiency of the PBDT2FT:PCBM solar cells decreased dramatically with the increasing length of the donor side chain, while the quantum efficiency of the PBDT2FT:ITIC solar cell was independent of the side chain length of the donor material. The difference in the quantum efficiency was ascribed to a difference in the effect of the length of the donor side chain on the morphology of the fullerene and non-fullerene systems, which suggests that the mechanism for the morphology evolution is different in the

non-fullerene system, possibly due to the lack of structural symmetry of the ITIC molecule compared to PCBM. Further studies revealed that in ITIC-based blended thin films the donor polymers with different side chains also had a similar coherence length of $\pi-\pi$ stacking, crystal size, and domain purity, giving rise to the similar internal quantum efficiency and PCE of the solar cells based on ITIC. As rational control over morphology is important to further optimize device performance, it is of interest to determine the parameters that do affect the domains size of the ITIC-based cells.

■ ASSOCIATED CONTENT

Ⓢ Supporting Information

The Supporting Information is available free of charge on the ACS Publications website at DOI: 10.1021/acs.macromol.6b01326.

> Materials and measurements, synthesis of the monomers and polymers, DFT calculations, GPC, CV measurement, FETs, solar cells, SCLC measurement, TEM images, and NMR spectra (PDF)

■ AUTHOR INFORMATION

Corresponding Authors
*E-mail: licheng1987@iccas.ac.cn (L.C.).
*E-mail: liweiwei@iccas.ac.cn (W.L.).
*E-mail: zheng.tang@iapp.de (Z.T.).
*E-mail: msewma@xjtu.edu.cn (W.M.).

Notes
The authors declare no competing financial interest.

■ ACKNOWLEDGMENTS

■ REFERENCES

(1) Lin, Y.; Zhan, X. Oligomer Molecules for Efficient Organic Photovoltaics. *Acc. Chem. Res.* **2016**, *49*, 175−183.

(2) Benten, H.; Mori, D.; Ohkita, H.; Ito, S. Recent Research Progress of Polymer Donor/Polymer Acceptor Blend Solar Cells. *J. Mater. Chem. A* **2016**, *4*, 5340−5365.

(3) Guo, X.; Facchetti, A.; Marks, T. J. Imide- and Amide-Functionalized Polymer Semiconductors. *Chem. Rev.* **2014**, *114*, 8943−9021.

(4) Zhan, C.; Yao, J. More than Conformational "Twisting" or "Coplanarity": Molecular Strategies for Designing High-Efficiency Nonfullerene Organic Solar Cells. *Chem. Mater.* **2016**, *28*, 1948−1964.

(5) Facchetti, A. Polymer Donor−Polymer Acceptor (all-Polymer) Solar Cells. *Mater. Today* **2013**, *16*, 123−132.

(6) Nielsen, C. B.; Holliday, S.; Chen, H.-Y.; Cryer, S. J.; McCulloch, I. Non-Fullerene Electron Acceptors for Use in Organic Solar Cells. *Acc. Chem. Res.* **2015**, *48*, 2803−2812.

(7) McAfee, S. M.; Topple, J. M.; Hill, I. G.; Welch, G. C. Key Components to the Recent Performance Increases of Solution Processed Non-Fullerene Small Molecule Acceptors. *J. Mater. Chem. A* **2015**, *3*, 16393−16408.

(8) Zhan, X.; Tan, Z. A.; Domercq, B.; An, Z.; Zhang, X.; Barlow, S.; Li, Y.; Zhu, D.; Kippelen, B.; Marder, S. R. A High-Mobility Electron-Transport Polymer with Broad Absorption and Its Use in Field-Effect Transistors and All-Polymer Solar Cells. *J. Am. Chem. Soc.* **2007**, *129*, 7246−7247.

(9) Li, S.; Zhang, H.; Zhao, W.; Ye, L.; Yao, H.; Yang, B.; Zhang, S.; Hou, J. Green-Solvent-Processed All-Polymer Solar Cells Containing a Perylene Diimide-Based Acceptor with an Efficiency over 6.5%. *Adv. Energy Mater.* **2016**, *6*, 1501991.

(10) Gao, L.; Zhang, Z.-G.; Xue, L.; Min, J.; Zhang, J.; Wei, Z.; Li, Y. All-Polymer Solar Cells Based on Absorption-Complementary Polymer Donor and Acceptor with High Power Conversion Efficiency of 8.27%. *Adv. Mater.* **2016**, *28*, 1884−1890.

(11) Long, X.; Ding, Z.; Dou, C.; Zhang, J.; Liu, J.; Wang, L. Polymer Acceptor Based on Double B←N Bridged Bipyridine (BNBP) Unit for High-Efficiency All-Polymer Solar Cells. *Adv. Mater.* **2016**, *28*, 6504.

(12) Li, W.; Roelofs, W. S. C.; Turbiez, M.; Wienk, M. M.; Janssen, R. A. J. Polymer Solar Cells with Diketopyrrolopyrrole Conjugated Polymers as the Electron Donor and Electron Acceptor. *Adv. Mater.* **2014**, *26*, 3304−3309.

(13) Holliday, S.; Ashraf, R. S.; Nielsen, C. B.; Kirkus, M.; Röhr, J. A.; Tan, C.-H.; Collado-Fregoso, E.; Knall, A.-C.; Durrant, J. R.; Nelson, J.; McCulloch, I. A Rhodanine Flanked Nonfullerene Acceptor for Solution-Processed Organic Photovoltaics. *J. Am. Chem. Soc.* **2015**, *137*, 898−904.

(14) Kwon, O. K.; Uddin, M. A.; Park, J.-H.; Park, S. K.; Nguyen, T. L.; Woo, H. Y.; Park, S. Y. A High Efficiency Nonfullerene Organic Solar Cell with Optimized Crystalline Organizations. *Adv. Mater.* **2016**, *28*, 910−916.

(15) Meng, D.; Sun, D.; Zhong, C.; Liu, T.; Fan, B.; Huo, L.; Li, Y.; Jiang, W.; Choi, H.; Kim, T.; Kim, J. Y.; Sun, Y.; Wang, Z.; Heeger, A. J. High-Performance Solution-Processed Non-Fullerene Organic Solar Cells Based on Selenophene-Containing Perylene Bisimide Acceptor. *J. Am. Chem. Soc.* **2016**, *138*, 375−380.

(16) Zhong, Y.; Trinh, M. T.; Chen, R.; Purdum, G. E.; Khlyabich, P. P.; Sezen, M.; Oh, S.; Zhu, H.; Fowler, B.; Zhang, B.; Wang, W.; Nam, C.-Y.; Sfeir, M. Y.; Black, C. T.; Steigerwald, M. L.; Loo, Y.-L.; Ng, F.; Zhu, X. Y.; Nuckolls, C. Molecular Helices as Electron Acceptors in High-Performance Bulk Heterojunction Solar Cells. *Nat. Commun.* **2015**, *6*, 8242.

(17) Hartnett, P. E.; Timalsina, A.; Matte, H. S. S. R.; Zhou, N.; Guo, X.; Zhao, W.; Facchetti, A.; Chang, R. P. H.; Hersam, M. C.; Wasielewski, M. R.; Marks, T. J. Slip-Stacked Perylenediimides as an Alternative Strategy for High Efficiency Nonfullerene Acceptors in Organic Photovoltaics. *J. Am. Chem. Soc.* **2014**, *136*, 16345−16356.

(18) Zang, Y.; Li, C.-Z.; Chueh, C.-C.; Williams, S. T.; Jiang, W.; Wang, Z.-H.; Yu, J.-S.; Jen, A. K. Y. Integrated Molecular, Interfacial, and Device Engineering towards High-Performance Non-Fullerene Based Organic Solar Cells. *Adv. Mater.* **2014**, *26*, 5708−5714.

(19) Li, H. Y.; Earmme, T.; Ren, G. Q.; Saeki, A.; Yoshikawa, S.; Murari, N. M.; Subramaniyan, S.; Crane, M. J.; Seki, S.; Jenekhe, S. A. Beyond Fullerenes: Design of Nonfullerene Acceptors for Efficient Organic Photovoltaics. *J. Am. Chem. Soc.* **2014**, *136*, 14589−14597.

(20) Hwang, Y. J.; Courtright, B. A. E.; Ferreira, A. S.; Tolbert, S. H.; Jenekhe, S. A. 7.7% Efficient All-Polymer Solar Cells. *Adv. Mater.* **2015**, *27*, 4578−4584.

(21) Hwang, Y.-J.; Li, H.; Courtright, B. A. E.; Subramaniyan, S.; Jenekhe, S. A. Nonfullerene Polymer Solar Cells with 8.5% Efficiency Enabled by a New Highly Twisted Electron Acceptor Dimer. *Adv. Mater.* **2016**, *28*, 124−131.

(22) Lin, Y.; Wang, J.; Zhang, Z.-G.; Bai, H.; Li, Y.; Zhu, D.; Zhan, X. An Electron Acceptor Challenging Fullerenes for Efficient Polymer Solar Cells. *Adv. Mater.* **2015**, *27*, 1170−1174.

(23) Lin, Y.; Zhang, Z.-G.; Bai, H.; Wang, J.; Yao, Y.; Li, Y.; Zhu, D.; Zhan, X. High-Performance Fullerene-Free Polymer Solar Cells with 6.31% Efficiency. *Energy Environ. Sci.* **2015**, *8*, 610−616.

(24) Lin, H.; Chen, S.; Li, Z.; Lai, J. Y. L.; Yang, G.; McAfee, T.; Jiang, K.; Li, Y.; Liu, Y.; Hu, H.; Zhao, J.; Ma, W.; Ade, H.; Yan, H. High-Performance Non-Fullerene Polymer Solar Cells Based on a Pair of Donor−Acceptor Materials with Complementary Absorption Properties. *Adv. Mater.* **2015**, *27*, 7299−7304.

(25) Li, Y.; Liu, X.; Wu, F.-P.; Zhou, Y.; Jiang, Z.-Q.; Song, B.; Xia, Y.; Zhang, Z.-G.; Gao, F.; Inganas, O.; Li, Y.; Liao, L.-S. Non-Fullerene Acceptor with Low Energy Loss and High External Quantum Efficiency: Towards High Performance Polymer Solar Cells. *J. Mater. Chem. A* **2016**, *4*, 5890−5897.

(26) Lin, Y.; He, Q.; Zhao, F.; Huo, L.; Mai, J.; Lu, X.; Su, C.-J.; Li, T.; Wang, J.; Zhu, J.; Sun, Y.; Wang, C.; Zhan, X. A Facile Planar Fused-Ring Electron Acceptor for As-Cast Polymer Solar Cells with 8.71% Efficiency. *J. Am. Chem. Soc.* **2016**, *138*, 2973−2976.

(27) Lin, Y.; Zhao, F.; He, Q.; Huo, L.; Wu, Y.; Parker, T. C.; Ma, W.; Sun, Y.; Wang, C.; Zhu, D.; Heeger, A. J.; Marder, S. R.; Zhan, X. High-Performance Electron Acceptor with Thienyl Side Chains for Organic Photovoltaics. *J. Am. Chem. Soc.* **2016**, *138*, 4955−4961.

(28) Bin, H.; Zhang, Z.-G.; Gao, L.; Chen, S.; Zhong, L.; Xue, L.; Yang, C.; Li, Y. Non-Fullerene Polymer Solar Cells Based on Alkylthio and Fluorine Substituted 2D-Conjugated Polymers Reach 9.5% Efficiency. *J. Am. Chem. Soc.* **2016**, *138*, 4657−4664.

(29) Yao, H.; Yu, R.; Shin, T. J.; Zhang, H.; Zhang, S.; Jang, B.; Uddin, M. A.; Woo, H. Y.; Hou, J. A Wide Bandgap Polymer with Strong π−π Interaction for Efficient Fullerene-Free Polymer Solar Cells. *Adv. Energy Mater.* **2016**, *6*, 1600742.

(30) Zhang, S.; Qin, Y.; Uddin, M. A.; Jang, B.; Zhao, W.; Liu, D.; Woo, H. Y.; Hou, J. A Fluorinated Polythiophene Derivative with Stabilized Backbone Conformation for Highly Efficient Fullerene and Non-Fullerene Polymer Solar Cells. *Macromolecules* **2016**, *49*, 2993−3000.

(31) Zhao, W.; Qian, D.; Zhang, S.; Li, S.; Inganäs, O.; Gao, F.; Hou, J. Fullerene-Free Polymer Solar Cells with over 11% Efficiency and Excellent Thermal Stability. *Adv. Mater.* **2016**, *28*, 4734−4739.

(32) Zhao, J.; Li, Y.; Yang, G.; Jiang, K.; Lin, H.; Ade, H.; Ma, W.; Yan, H. Efficient Organic Solar Cells Processed from Hydrocarbon Solvents. *Nat. Energy* **2016**, *1*, 15027.

(33) Kim, T.; Kim, J.-H.; Kang, T. E.; Lee, C.; Kang, H.; Shin, M.; Wang, C.; Ma, B.; Jeong, U.; Kim, T.-S.; Kim, B. J. Flexible, Highly Efficient All-Polymer Solar Cells. *Nat. Commun.* **2015**, *6*, 8547.

(34) Huang, Y.; Kramer, E. J.; Heeger, A. J.; Bazan, G. C. Bulk Heterojunction Solar Cells: Morphology and Performance Relationships. *Chem. Rev.* **2014**, *114*, 7006.

(35) Dou, L.; You, J.; Hong, Z.; Xu, Z.; Li, G.; Street, R. A.; Yang, Y. 25th Anniversary Article: A Decade of Organic/Polymeric Photovoltaic Research. *Adv. Mater.* **2013**, *25*, 6642−6671.

(36) Leclerc, N.; Chávez, P.; Ibraikulov, O.; Heiser, T.; Lévêque, P. Impact of Backbone Fluorination on π-Conjugated Polymers in Organic Photovoltaic Devices: A Review. *Polymers* **2016**, *8*, 11.

(37) Liu, Y.; Zhao, J.; Li, Z.; Mu, C.; Ma, W.; Hu, H.; Jiang, K.; Lin, H.; Ade, H.; Yan, H. Aggregation and Morphology Control Enables Multiple Cases of High-Efficiency Polymer Solar Cells. *Nat. Commun.* **2014**, *5*, 5293.

(38) Price, S. C.; Stuart, A. C.; Yang, L.; Zhou, H.; You, W. Fluorine Substituted Conjugated Polymer of Medium Band Gap Yields 7% Efficiency in Polymer–Fullerene Solar Cells. *J. Am. Chem. Soc.* **2011**, *133*, 4625−4631.

(39) Chen, H. Y.; Hou, J. H.; Zhang, S. Q.; Liang, Y. Y.; Yang, G. W.; Yang, Y.; Yu, L. P.; Wu, Y.; Li, G. Polymer Solar Cells with Enhanced Open-Circuit Voltage and Efficiency. *Nat. Photonics* **2009**, *3*, 649−653.

(40) Scharber, M. C.; Koppe, M.; Gao, J.; Cordella, F.; Loi, M. A.; Denk, P.; Morana, M.; Egelhaaf, H.-J.; Forberich, K.; Dennler, G.; Gaudiana, R.; Waller, D.; Zhu, Z.; Shi, X.; Brabec, C. J. Influence of the Bridging Atom on the Performance of a Low-Bandgap Bulk Heterojunction Solar Cell. *Adv. Mater.* **2010**, *22*, 367−370.

(41) Dou, L.; Chang, W.-H.; Gao, J.; Chen, C.-C.; You, J.; Yang, Y. A Selenium-Substituted Low-Bandgap Polymer with Versatile Photovoltaic Applications. *Adv. Mater.* **2013**, *25*, 825−831.

(42) Vohra, V.; Kawashima, K.; Kakara, T.; Koganezawa, T.; Osaka, I.; Takimiya, K.; Murata, H. Efficient Inverted Polymer Solar Cells Employing Favourable Molecular Orientation. *Nat. Photonics* **2015**, *9*, 403−408.

(43) Meager, I.; Ashraf, R. S.; Mollinger, S.; Schroeder, B. C.; Bronstein, H.; Beatrup, D.; Vezie, M. S.; Kirchartz, T.; Salleo, A.; Nelson, J.; McCulloch, I. Photocurrent Enhancement from Diketopyrrolopyrrole Polymer Solar Cells through Alkyl-Chain Branching Point Manipulation. *J. Am. Chem. Soc.* **2013**, *135*, 11537−11540.

(44) Li, W.; Hendriks, K. H.; Furlan, A.; Roelofs, W. S. C.; Meskers, S. C. J.; Wienk, M. M.; Janssen, R. A. J. Effect of the Fibrillar Microstructure on the Efficiency of High Molecular Weight Diketopyrrolopyrrole-Based Polymer Solar Cells. *Adv. Mater.* **2014**, *26*, 1565−1570.

(45) Mandoc, M. M.; Veurman, W.; Koster, L. J. A.; de Boer, B.; Blom, P. W. M. Origin of the Reduced Fill Factor and Photocurrent in MDMO-PPV:PCNEPV All-Polymer Solar Cells. *Adv. Funct. Mater.* **2007**, *17*, 2167−2173.

(46) Xue, L. J.; Zhang, J. L.; Han, Y. C. Phase Separation Induced Ordered Patterns in Thin Polymer Blend Films. *Prog. Polym. Sci.* **2012**, *37*, 564−594.

(47) Zhou, H. X.; Yang, L. Q.; Stoneking, S.; You, W. A Weak Donor-Strong Acceptor Strategy to Design Ideal Polymers for Organic Solar Cells. *ACS Appl. Mater. Interfaces* **2010**, *2*, 1377−1383.

(48) Hedström, S.; Wang, E.; Persson, P. Defining Donor and Acceptor Strength in Conjugated Copolymers. *Mol. Phys.* **2016**, 1−12.

(49) Fei, Z.; Boufflet, P.; Wood, S.; Wade, J.; Moriarty, J.; Gann, E.; Ratcliff, E. L.; McNeill, C. R.; Sirringhaus, H.; Kim, J.-S.; Heeney, M. Influence of Backbone Fluorination in Regioregular Poly(3-alkyl-4-fluoro)thiophenes. *J. Am. Chem. Soc.* **2015**, *137*, 6866−6879.

(50) Li, W.; Hendriks, K. H.; Furlan, A.; Wienk, M. M.; Janssen, R. A. J. High Quantum Efficiencies in Polymer Solar Cells at Energy Losses below 0.6 eV. *J. Am. Chem. Soc.* **2015**, *137*, 2231−2234.

(51) Zimmermann, E.; Ehrenreich, P.; Pfadler, T.; Dorman, J. A.; Weickert, J.; Schmidt-Mende, L. Erroneous Efficiency Reports Harm Organic Solar Cell Research. *Nat. Photonics* **2014**, *8*, 669−672.

(52) Lu, Z.; Jiang, B.; Zhang, X.; Tang, A.; Chen, L.; Zhan, C.; Yao, J. Perylene−Diimide Based Non-Fullerene Solar Cells with 4.34% Efficiency through Engineering Surface Donor/Acceptor Compositions. *Chem. Mater.* **2014**, *26*, 2907−2914.